

Active load control for wind turbine blades using trailing edge flap

Jong-Won Lee¹, Joong-Kwan Kim¹, Jae-Hung Han*¹ and Hyung-Kee Shin²

¹Department of Aerospace Engineering, KAIST, Daejeon, 305-600, Korea

²Korea Institute of Energy Research, Daejeon, 305-343, Korea

(Received September 22, 2011, Revised March 27, 2012, Accepted April 2, 2012)

Abstract. The fatigue load of a turbine blade has become more important because the size of commercial wind turbines has increased dramatically in the past 30 years. The reduction of the fatigue load can result in an increase in operational efficiency. This paper numerically investigates the load reduction of large wind turbine blades using active aerodynamic load control devices, namely trailing edge flaps. The PD and LQG controllers are used to determine the trailing edge flap angle; the difference between the root bending moment and its mean value during turbulent wind conditions is used as the error signal of the controllers. By numerically analyzing the effect of the trailing edge flaps on the wind turbines, a reduction of 30-50% in the standard deviation of the root bending moment was achieved. This result implies a reduction in the fatigue damage on the wind turbines, which allows the turbine blade lengths to be increased without exceeding the designed fatigue damage limit.

Keywords: wind turbine blade; load reduction; fatigue; smart control; trailing edge flap

1. Introduction

The size of commercial wind turbines has increased dramatically in the past 30 years from rated power specification of approximately 50 kW and rotor diameters of 10-15 m to the current 5 MW machines with a rotor diameter of more than 120 m. The ultimate goal of much research in the field of wind turbines has been to lower the operational cost per kWh. For the large wind turbines, reducing the load on the blades is an effective method of reducing the cost of energy generation. Reducing the blade load not only lowers the cost of the blades themselves, but also reduces the loads on other components such as the drive train and tower. Fatigue load is a key factor in the design of wind turbine blades. The reduction of the fatigue load can result in increased component lifetimes, reduced maintenance requirements, and overall lower costs.

With the increasing size of wind turbines, the need for more advanced load controls has increased. With the implementation of active aerodynamic load control devices, such controls should be attainable. These load control devices, in combination with sensors, controllers, and actuators, enable the desired control over the blades. This concept is generally referred to as 'smart rotor control'. Among the proposed aerodynamic load control devices, trailing edge flaps have been considered one of the most feasible and efficient solutions.

*Corresponding author, Professor, Ph.D., E-mail: jaehunghan@kaist.ac.kr

Troldborg (2005) investigated the effect of the size and shape of the variable trailing edge geometry on the active control performance. Basualdo (2005) developed a 2D aeroelastic model based on a panel method for an airfoil with a deformable trailing edge. Gaunaa (2006) developed an analytical model for the unsteady force on the variable geometry thin airfoil using potential flow. Bergami (2008) described the unsteady aerodynamic behavior of the flap equipped airfoil that allows the computation of the aerodynamic forces and their distribution for a 2D airfoil undergoing arbitrary motion and deformation of the camberline. Wilson *et al.* (2009) performed numerical simulations using the trailing edge flaps as active aerodynamic load control devices in a wind turbine with 5 MW rated power. A 20-32% reduction in the blade root flap bending moments was achieved. Barlas *et al.* (2009) developed a comprehensive aeroelastic model that can investigate the active flap concepts on the Upwind 5 MW wind turbine. For the flapped sections, a 2D unsteady aerodynamic model is used, based on work of helicopter aerodynamics, as described by Leishman. The previous research has demonstrated the potential of active load control through flaps or variable geometry trailing edge airfoils for load reductions in the wind turbine blades. Furthermore, Anderson (2007) performed wind tunnel tests to investigate the potential of active load control through variable trailing edge geometry.

This study investigates load reduction on trailing edge flaps (TEFs) in the operation of the NREL 5 MW wind turbine and the KIER 3 MW wind turbine. An aeroelastic analysis method was developed; the unsteady aerodynamic model has been implemented using the Modified Strip Theory (Kim 2011); the structural model of the blades has been established using MSC.ADAMS and ANSYS. PD the LQG controllers are used with the blade root bending moment as the feedback signal and the TEF deflection angle as the control input. The blade load controls in a normal turbulence model are shown for these control schemes.

2. Modeling

2.1 Wind turbine model

The wind turbine models used for the rotor control analysis are the NREL 5 MW wind turbine (Jonkman 2009) and the KIER 3 MW wind turbine. The NREL wind turbine has a 126 m diameter rotor with 61.5 m long blades. The KIER wind turbine is a pitch regulated wind turbine with a hub height of 80 m. The KIER model has a three-bladed rotor of 91 m diameter with 44 m long blades; the KIER wind turbine model was developed by the Korea Institute of Energy Research (KIER). This rotor is positioned upwind with a clockwise rotation direction, viewed downwind. The properties and operation conditions of the KIER model are summarized in Table 1.

2.2 Aeroelastic analysis model

The aerodynamic model in this study is based on the modified strip theory (MST), which was originally proposed by De Laurier (1993) for the flapping wing aerodynamic model. The total lift and thrust are obtained by integrating the sectional aerodynamic forces calculated in each section as shown in Fig. 1. Kim (2011) improved the original MST in order to consider a higher resultant angle of attack, and extended the dynamic stall model for not only pitching motion but also plunging motion. This study employs the improved MST after further modification for wind turbine blades. This computationally efficient aerodynamic model is particularly applicable to the

Table 1 Characteristics of the KIER wind turbine

Rated power	3 MW
Number of blades	3
Rotor diameter	91.3 m
Blade length	44 m
Hub height	80 m
Cut-in, rated, cut-out wind speed	3, 11, 25 m/s
Cut-in, cut-out rotor speed	8, 15.7 rpm
Rotor mass	58460 kg
Mass of nacelle and rotor	133500 kg
Tower mass	191700 kg
Overall mass	325100 kg

design and performance prediction of wind turbine blades and time-consuming fluid-structure interaction analyses.

The MST modified for wind turbine blades is described briefly in this paper. The aerodynamic forces of each section of a wind turbine blade can be represented as shown in Figs. 1 and 2 shows the aerodynamic forces and motion variables for a particular section of the blade. If the leading edge of the blade section is treated as a reference point, then the section's motion consists of the free stream speed U , rotating speed Ωr , plunging motion \dot{h} , and pitching motion $\dot{\theta}$.

The section's normal force (dN_c) generated by the circulation ($d\Gamma$) around the blade can be expressed as

$$dN_c = 2\pi(\alpha' + \alpha_0) \cos \gamma \frac{\rho UV}{2} c dy \quad (1)$$

where ρ , U , and α_0 are the atmospheric density, free stream speed, and angle of the section's zero-lift line, respectively. The angle of attack, α' , the resultant flow velocity at 1/4 chord location, V , and the relative angle of attack, γ , can be expressed as follows

$$\alpha' = \frac{ARC'(k)\alpha - 2\alpha_0}{2 + AR} \quad (2)$$

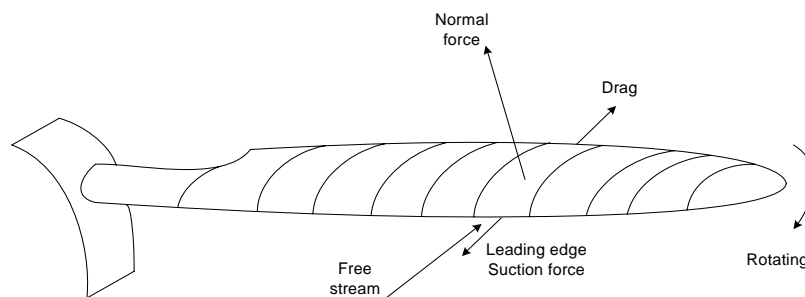


Fig. 1 Wind turbine blade and aerodynamic forces

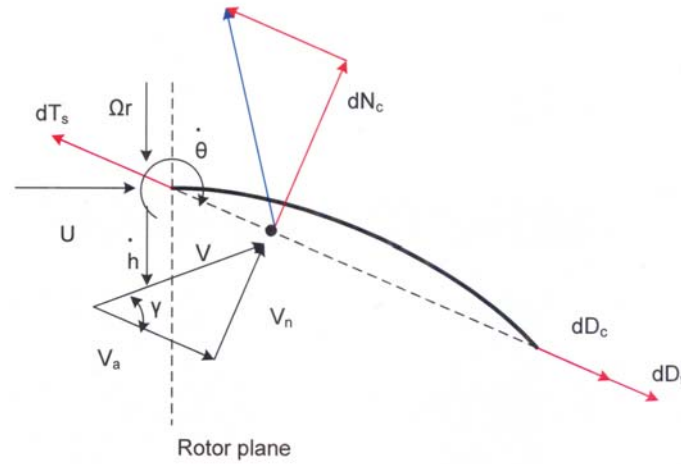


Fig. 2 Section aerodynamic forces and motion variables

$$V = \left[\left(U \cos \theta + \dot{h} \sin \theta + \Omega r \sin \theta \right)^2 + \left(U \sin \theta - \dot{h} \cos \theta - \Omega r \cos \theta + 0.25c\dot{\theta} \right)^2 \right]^{1/2} \quad (3)$$

$$\gamma = \tan^{-1} \left[\frac{U \sin \theta - \dot{h} \cos \theta - \Omega r \cos \theta + 0.25c\dot{\theta}}{U \cos \theta + \dot{h} \sin \theta + \Omega r \sin \theta} \right] \quad (4)$$

where AR , c , and k are the aspect ratio, chord, and reduced frequency, respectively. The other aerodynamic forces of the wing section shown in Fig. 2 can be expressed as follows

$$dN_a = \frac{\rho \pi c^2}{4} \dot{v}_2 dy \quad (5)$$

$$dD_c = -2\pi \alpha_0(\alpha') \cos \gamma \frac{\rho UV}{2} c dy \quad (6)$$

$$dT_s = \eta_s 2\pi \left(\alpha' - \frac{1}{4} \frac{c\dot{\theta}}{U} \right) \sin \gamma \frac{\rho UV}{2} c dy \quad (7)$$

$$dD_f = C_{d_f} \frac{\rho v_a^2}{2} c dy \quad (8)$$

where dN_a , dD_c , dT_s , and dD_f are the additional force due to the apparent mass, the chordwise force due to the camber, the leading edge suction force, and the chordwise friction drag due to

viscosity, respectively. The mid-chord normal velocity can be expressed as

$$v_2 = U \sin \theta - (\dot{h} + \Omega r) \cos \theta + 0.5c\dot{\theta} \quad (9)$$

When the flow condition is out of the attached flow, it is assumed that the flow is completely separated and all chordwise forces are negligible (localized post stall behavior). The normal forces in the stall condition are given by

$$(dN_c)_{sep} = (C_{d_c}) \frac{\rho \hat{V} V_n}{2} c dy \quad (10)$$

$$(dN_a)_{sep} = \frac{\rho \pi c^2}{8} \dot{v}_2 dy \quad (11)$$

where \hat{V} and V_n are the resultant flow velocity and normal flow velocity at mid-chord location, respectively. Finally, the normal and horizontal forces of each section, $dN = dN_c + dN_a$ and $dF_a = dT_s - dD_c - dD_f$, can be obtained using Eqs. (1), (5)-(8), (10) and (11).

There have been proposed various structural modeling methods for the wind turbine blades (See Holm-Jørgensen 2008). In order to analyze the dynamic response of a flexible wind turbine blade, the modal flexibility method is used, in this study. The modal flexibility method, as used in MSC.ADAMS/Flex, is a method of modeling flexible bodies in multibody dynamics simulations. With this method, a limited set of mode shapes, or eigenvectors, is assigned to a flexible body. During the analysis, the relative amplitude of each eigenvector is calculated in each time step. Several modes are combined using the principles of the linear modal superposition to represent the total deformation of the body.

In order to model flexible bodies using the modal flexibility approach in MSC.ADAMS, these bodies are first created as a finite element (FE) model in ANSYS. Then, they are exported to a Modal Neutral Files (MNF). The information in the MNF includes geometry (node locations and node connectivity), nodal mass, nodal inertia, mode shapes, and the generalized mass and stiffness for the mode shapes.

The wind turbine blade FE model was constructed using the BEAM188 element. The density of the beam element was set to zero, because the rotary inertia properties of the beam elements around the blade pitch axis cannot be set manually, which results in incorrect torsion frequencies. Setting the density to zero not only results in massless elements, it also removes the internally calculated rotary inertia. Instead, the mass and inertia properties are represented using point mass elements (MASS21) attached to each node along the blade. As the point masses are directly attached to the nodes, these are positioned in the center of gravity in the blade sections. Modeling of the centripetal forces limits the modal flexibility implementation in ADAMS. In ADAMS the centripetal force of a rotating body is calculated for its center of gravity, which is then applied to the entire body. In this modeling method acceleration variations along the span of the rotating rotors are not accounted. In this research, the blades were divided into five sections in order to correctly model acceleration variation along the span of the rotor.

The aerodynamic model is included as a subroutine to the flexible multibody dynamics solver (MSC.ADAMS). The calculated blade sectional kinematic variables, such as the plunging and

pitching motions, are used as the input parameters for the aerodynamic model in order to calculate the instantaneous sectional aerodynamic loads. The fluid-structure interaction analysis was conducted by combining the flexible blade structural model and the improved MST.

2.3 Trailing edge flap model

The trailing edge flap (TEF) aerodynamic modeling is based on the thin airfoil theory for a flat airfoil with a flat trailing edge flap (Theodorsen 1935). The aerodynamic effects of the TEF are added to the aerodynamic forces on an airfoil determined by MST. For the NREL model, the TEFs are added to the blade platform from 70% to 90% span. For this section of the blade, the airfoil is a NACA 64618. The TEFs were chosen to have a 20% chord length, a deflection range of ± 20 degrees, and a deflection rate of 70 degrees per second. For the KIER model, the TEFs are added to the blade platform from 70% to 90% span. For this section of the blade, the airfoil is a KWA026 developed by KIER. The TEF specifications of the KIER model are the same as those for the NREL model.

3. TEF controller design

The goal of the TEF controller design is to minimize the blade root bending moment oscillations of the blade about its mean value during turbulent wind conditions. The blade root bending moment is used as the feedback signal and the TEF deflection angle is used as a control variable. PD and LQG controllers are employed in this study.

3.1 PD controller

A proportional-derivative (PD) controller is implemented in order to obtain load reduction. The difference between the measured root bending moment and the mean value of the nominal operation case without TEF control is used as the error signal for the controller. However, the actual structural dynamics of the TEF actuator are not considered. The control input is the TEF deflection angle and the control law becomes

$$\beta(t) = -K_p (M - M_{mean}) - K_d \frac{\partial M}{\partial t} \quad (12)$$

The minus error signal indicates a negative flap deflection (moving upwards) decreasing the lift. The PD control scheme is shown in Fig. 3.

The control gain is determined using the Ziegler-Nichols rules (Ogata 1990). The gain is obtained by simulating the response of the blade to a step input of an incoming flow velocity. A critical proportional gain enables the system to obtain sustained or divergent oscillations. The suggested proportional gain, which is a half of the critical proportional gain, stabilizes the system

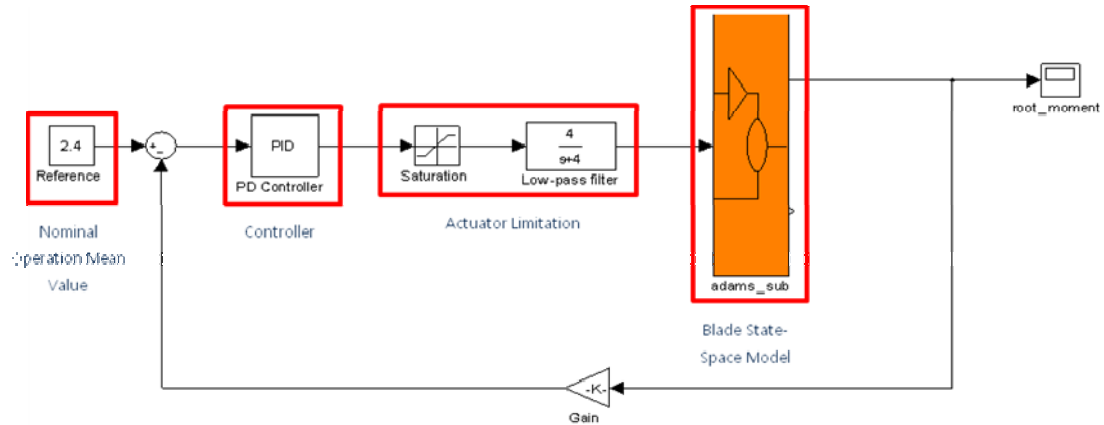


Fig. 3 Flap PD control scheme for wind turbine blade

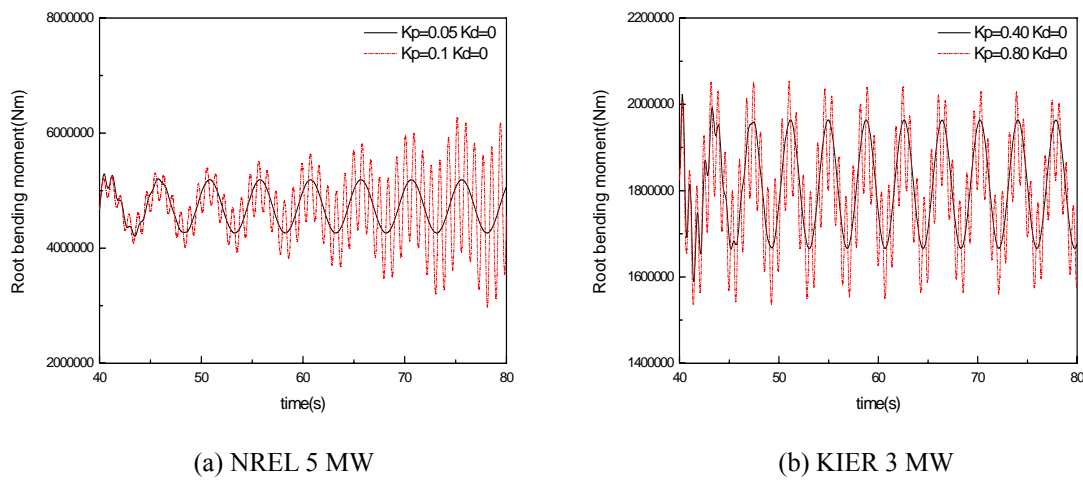


Fig. 4 Response to the step change in incoming flow velocity with proportional control only

as shown in Fig. 4. The simulation conditions for the PD controller gain tuning and the PD gains used in the simulation are shown in Table 2.

3.2 LQG controller

In order to design a TEF optimal controller using a model-based control design framework, a closed-form model of the wind turbine system is essential. In this work, the Prediction Error Method (PEM) (Ljung 2001 and Soderstrom 1989) is used to obtain the closed-form system model of the two wind turbines.

The PEM is a system parameter estimation method using iterative prediction-error minimization. By using input/output datasets of a target system, a black box system model (Eq. (13)) can be obtained. In general, an input with a wide bandwidth (impulse, step, random signal) is

used for the system excitation. In order to generate datasets for the PEM, an impulse or a step signal to the TEF deflection angle is used as the system input, and the corresponding root bending moment and flap-wise tip deflection are used as outputs.

$$\begin{aligned}\mathbf{x}_{r \times 1}[n+1] &= A_{r \times r} \mathbf{x}_{r \times 1}[n] + B_{r \times s} \mathbf{u}_{s \times 1}[n] + K_{r \times q} \mathbf{e}_{q \times 1}[n] \\ \mathbf{y}_{q \times 1}[n] &= C_{q \times r} \mathbf{x}_{r \times 1}[n] + D_{q \times s} \mathbf{u}_{s \times 1}[n] + \mathbf{e}_{q \times 1}[n]\end{aligned}$$

where:

$\mathbf{x}_{r \times 1}$: system states

$\mathbf{y}_{q \times 1}$: outputs of the system

$\mathbf{u}_{s \times 1}$: control inputs

$\mathbf{e}_{q \times 1}$: Gaussian white noise vector

(13)

Table 2 Simulation conditions for the PD controller gain tuning and PD controller gain

Model	Wind Condition (Step input)	K_p	K_d
NREL	11.5 → 13.5 m/s	0.05	0.003
KIER	11 → 13 m/s	0.4	0.02

Let $Z^N = \{(\mathbf{u}_{s \times 1}[1], \mathbf{y}_{q \times 1}[1]), (\mathbf{u}_{s \times 1}[2], \mathbf{y}_{q \times 1}[2]), \dots, (\mathbf{u}_{s \times 1}[N], \mathbf{y}_{q \times 1}[N])\}$ input/output datasets recorded from the response of the wind turbine system in a discretized time window. The general predictor model in terms of ξ (an arbitrary parameter vector) can be defined as

$$\hat{\mathbf{y}}[n | \xi] = f(Z^{n-1}, \xi) \quad (14)$$

An estimate of ξ (Eq. (15(a))) can be obtained from the model parameterization and recorded datasets. This process is achieved through minimizing the prediction error, $\varepsilon = \mathbf{y}(n) - \hat{\mathbf{y}}(n | \xi)$, with a squared Euclidian norm (Eq. (15(b))).

$$\hat{\xi}_N = \arg \min_{\xi} \{V_N(\xi)\} \quad (15a)$$

$$V_N(\xi) = \sum_{n=1}^N \|\mathbf{y}[n] - f(Z^{n-1}, \xi)\|^2 \quad (15b)$$

The optimal estimate of ξ is defined in Eq. (16), and the subscript “ r ” indicates the modeling order of the PEM. Generally, as the order of the PEM and the number of the input/output datasets

increase, the model parameterization of the system tends to be more accurate.

$$\hat{\xi}_N = (A_{r \times r}, B_{r \times s}, C_{q \times r}, D_{q \times s}, K_{r \times q}) \quad (16)$$

Note that the parameterized system model ($X_{r \times 1}$) in Eq. (13) has no physical interpretation, and it is called a hyperstate. The hyperstate only provides mapping between the inputs and outputs to the system and reproduces the arbitrary behaviors of the parameterized wind turbine system model.

The closed-form models of the wind turbine blade systems were obtained through the PEM. The system models are used to design a Linear Quadratic Regulator (LQR) control for TEF control. The LQR (Dorato 1995) is designed based on the output weighting matrix Q for minimizing the quadratic performance index, J_{LQRy} (Eq. (17))

$$J_{LQRy} = \sum_0^{\infty} \left\{ \mathbf{y}[n]^T Q_{LQRy} \mathbf{y}[n] + \mathbf{u}[n]^T R_{LQRy} \mathbf{u}[n] \right\} \quad (17)$$

The optimal regulating gain $K_{2 \times r}^{LQRy}$ is derived from the Algebraic Riccati Equation (ARE), and the regulating optimal control input according to the performance index (Eq. (17)) is given as

$$\mathbf{u}_{s \times 1}(t) = -K_{s \times r}^{LQRy} \mathbf{x}_{r \times 1}(t) \quad (18)$$

In order to design a LQG regulator, the Kalman optimal state estimator minimizing the state estimation error is required. It can also be obtained by solving the Filter Algebraic Riccati Equation (FARE) with noise covariance and the optimal state estimator is as follows

$$\begin{aligned} \hat{X}_{r \times 1}[n+1|n] &= (A_{r \times r} - L_{r \times q} C_{q \times r}) \hat{X}_{r \times 1}[n|n-1] + [B_{r \times s} L_{r \times q}] \begin{Bmatrix} u_{s \times 1}[n] \\ y_{q \times 1}[n] \end{Bmatrix} \\ \begin{Bmatrix} \hat{y}_{q \times 1}[n] \\ \hat{X}_{r \times 1}[n] \end{Bmatrix} &= \begin{bmatrix} C_{q \times r} (I_{r \times r} - M_{r \times q} C_{q \times r}) \\ I_{r \times r} - M_{r \times q} C_{q \times r} \end{bmatrix} \hat{X}_{r \times 1}[n|n-1] + \begin{bmatrix} C_{q \times r} M_{r \times q} \\ M_{r \times q} \end{bmatrix} y_{q \times 1}[n] \end{aligned} \quad (19)$$

The resulting LQG regulator has the following state-space equations

$$\begin{aligned} \hat{\mathbf{x}}_{r \times 1}[n+1|n] &= [A_{r \times r} - L_{r \times q} C_{q \times r} - B_{r \times s} K] \hat{\mathbf{x}}_{r \times 1}[n|n-1] + L_{r \times q} \mathbf{y}_{q \times 1}[n] \\ \mathbf{u}_{s \times 1}[n] &= -K_{s \times r}^{LQRy} \hat{\mathbf{x}}_{r \times 1}[n|n-1] \end{aligned} \quad (20)$$

A closed-form model of the NREL blades was obtained using the abovementioned PEM technique. A step input of 20 degrees was given to the TEF and the corresponding responses were recorded to create input/output datasets (Fig. 5(a)). These datasets were used to develop a 10th order PEM-based system model (fitness: 96%) for wind turbines.

An optimal full state feedback gain aims to minimize the quadratic performance index (Eq.

(21)). The LQR is combined with the Kalman optimal state estimator and formed LQG regulator in order to control the TEF in order to minimize the bending moment at the blade root.

A closed-form model of the KIER 3 MW wind turbine blade was also obtained from the PEM. An impulse input of 20 degrees was given to the TEF and the corresponding responses were recorded in order to create input/output datasets (Fig. 5(b)). These datasets were used to develop a sixth order PEM-based system model (fitness: 94%) for the wind turbine.

Similarly, an optimal full state feedback gain was found in order to minimize Eq. (22). For the KIER 3 MW wind turbine blade system, the weighting matrices (Q, R) demonstrated that the cost is more sensitive to the change of the root bending moment of the blade. A corresponding LQG regulator was also obtained for the TEF control of the KIER 3 MW wind turbine.

$$\begin{aligned}
 J_{LQR} &= \sum_0^{\infty} [\mathbf{y}^T[n]Q\mathbf{y}[n] + \mathbf{u}^T[n]R\mathbf{u}[n]] \\
 \mathbf{y}_{2 \times 1} &= \begin{bmatrix} \text{normalized blade tip deflection} \\ \text{normalized root bending moment} \end{bmatrix} \\
 \mathbf{u}_{1 \times 1} &= [\text{TEF control input}] \\
 Q &= \begin{bmatrix} 1 & 0 \\ 0 & 1 \end{bmatrix}, \quad R = [1]
 \end{aligned} \tag{21}$$

$$\begin{aligned}
 J_{LQR} &= \sum_0^{\infty} [\mathbf{y}^T[n]Q\mathbf{y}[n] + \mathbf{u}^T[n]R\mathbf{u}[n]] \\
 \mathbf{y}_{2 \times 1} &= \begin{bmatrix} \text{normalized blade tip deflection} \\ \text{normalized root bending moment} \end{bmatrix} \\
 \mathbf{u}_{1 \times 1} &= [\text{TEF control input}] \\
 Q &= \begin{bmatrix} 5 & 0 \\ 0 & 35 \end{bmatrix}, \quad R = [1]
 \end{aligned} \tag{22}$$

3.3 Simulation conditions

In order to evaluate the load reduction performance using the TEF under turbulent wind profiles, various simulations were performed. The turbulent wind profiles were generated by the TurboSim program developed by NREL. The wind conditions were defined using the Normal Turbulence Model (NTM) derived from the International Electrotechnical Commission (IEC) standards (IEC 61400-1 Ed.3). The simulation duration was 600 seconds and the other simulation conditions are shown in Table 3.

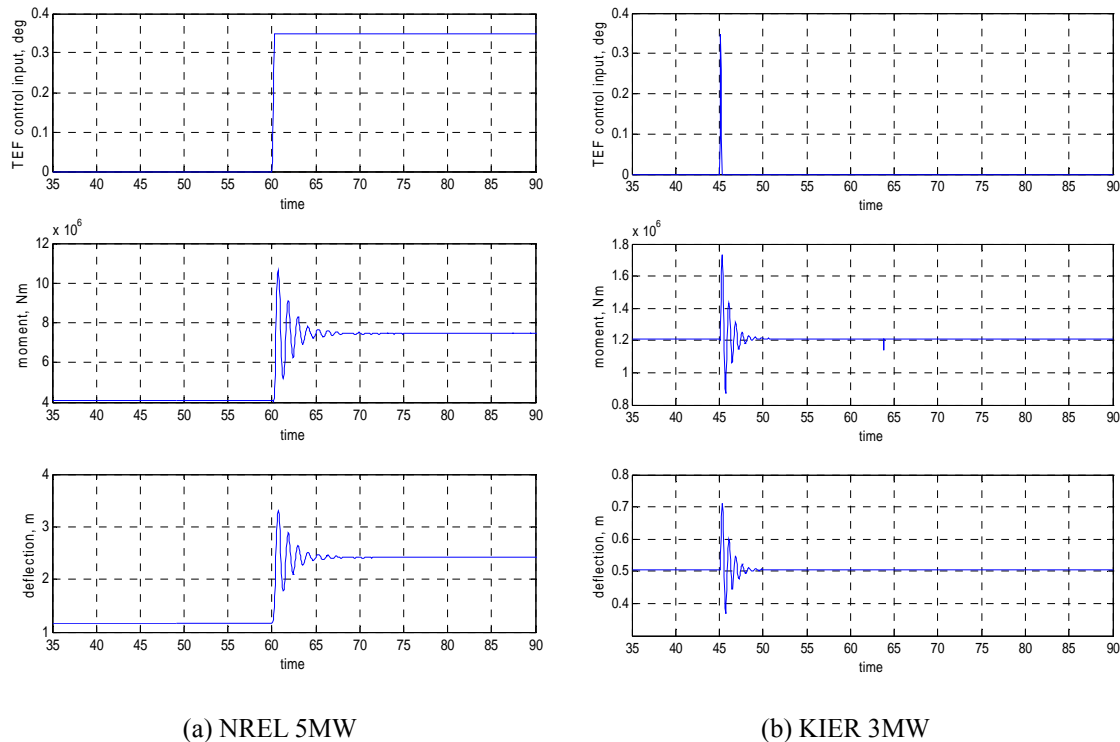


Fig. 5 Input/output datasets for wind turbine blade system

Table 3 Load control simulation conditions

Model	Wind condition (wind speed (rotating speed))
NREL	11.5 m/s (12 rpm)
	7 m/s (11 rpm)
KIER	11 m/s (15.7 rpm)
	15 m/s (15.7 rpm)

4. Numerical simulation results

4.1 NREL wind turbine

Fig. 6 illustrates the blade root bending moment over a 40 second period for both controlled and uncontrolled cases. When controlled, the root bending moment converges to the value of 4 MN-m, which is the overall average of the uncontrolled root bending moment. This effect is substantiated by the histograms below: when controlled, the values of the root bending moments are more densely distributed than the uncontrolled case (Fig. 7). Furthermore, as seen in Table 4, the standard deviation is reduced for the controlled case. This reduction in fluctuation signifies a reduction in fatigue loads. For the LQG controller, the standard deviation is reduced more compared with the PD controller. However, as seen in Fig. 8, the LQG necessitates a better

performing TEF actuator: the PD controller operates within ± 5 degrees while the LQG controller operates within ± 10 degrees.

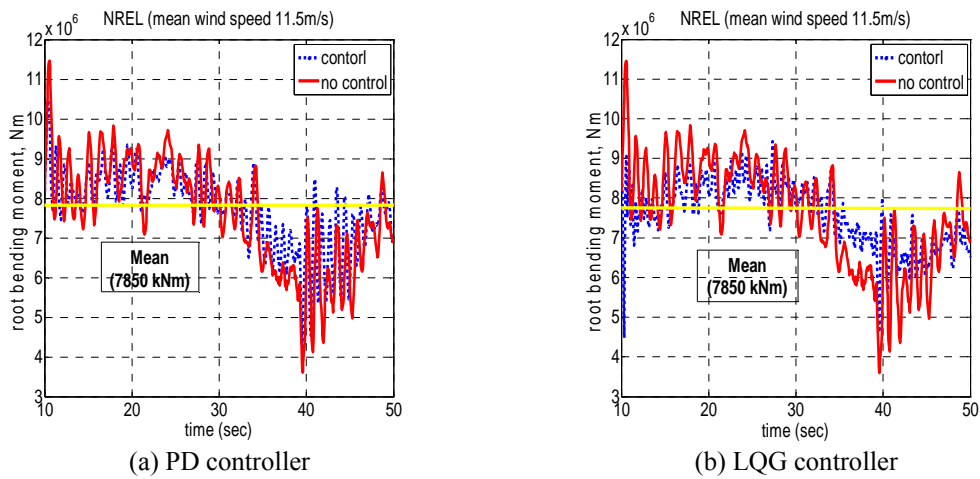


Fig. 6 Root bending moment of the NREL model at wind speed 11.5 m/s

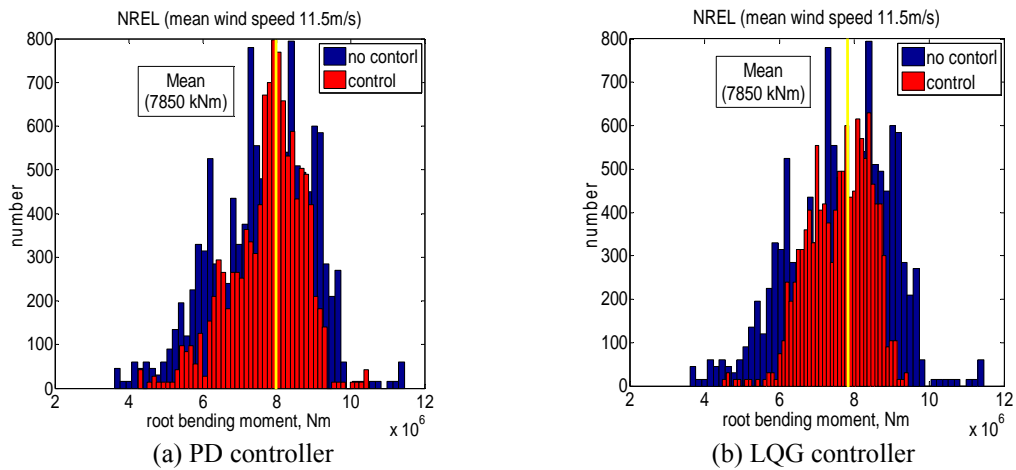


Fig. 7 Root bending moment histogram of the NREL model at wind speed 11.5 m/s

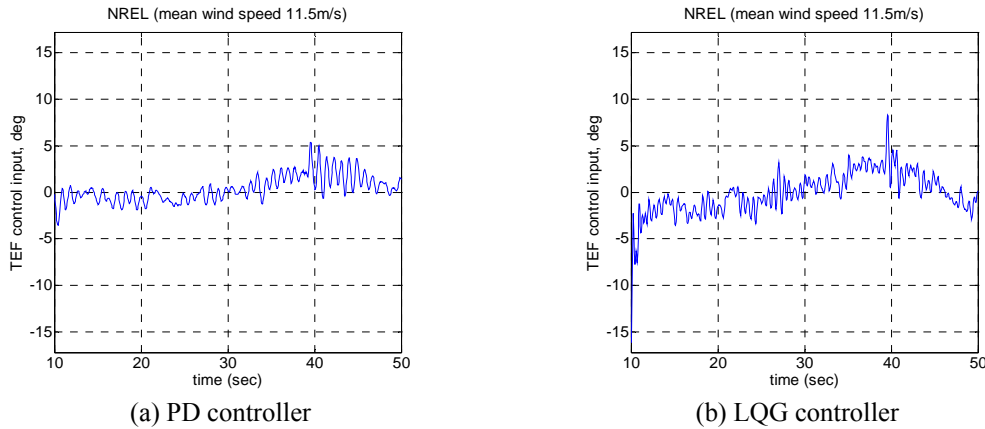


Fig. 8 TEF control input of the NREL model at wind speed 11.5 m/s

4.2 KIER wind turbine

From the three simulated wind conditions, the 11 m/s condition is shown. As seen in Fig. 9, the root bending moment converges to 2.4 MN-m in the controlled case. The histogram (Fig. 10) further accentuates this effect and graphically illustrates the narrow distribution of moments, signifying reduced fatigue loads. Table 5 shows a reduction in the standard deviation for both controllers. Moreover, the LQG controller also necessitates a better performing actuator (± 15 degrees) as seen in Fig. 11. Overall, the KIER model behaves very similarly to the NREL model.

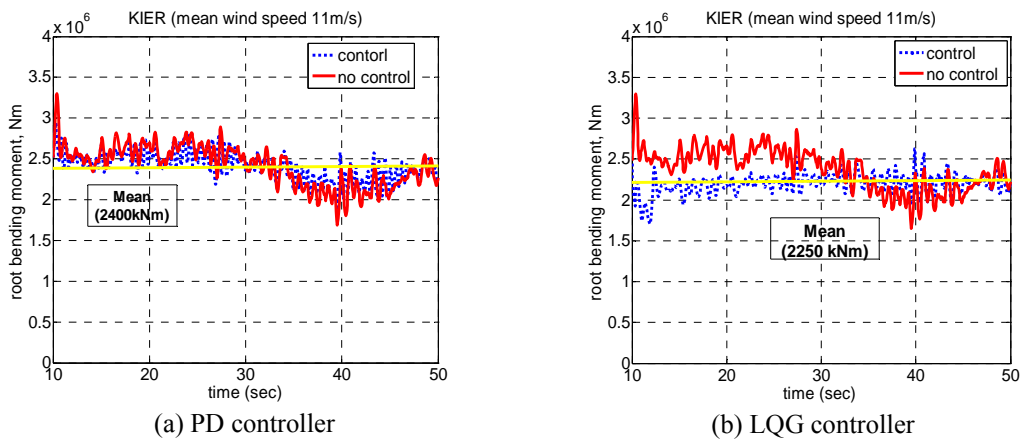


Fig. 9 Root bending moment of the KIER model at wind speed 11 m/s

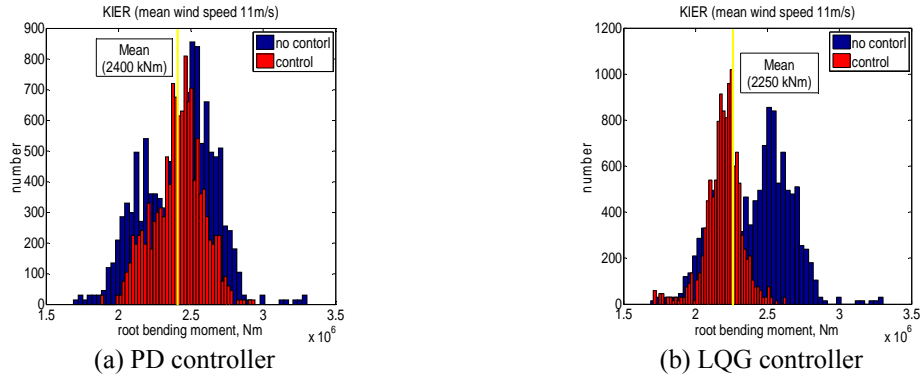


Fig. 10 Root bending moment histogram of the KIER model at wind speed 11 m/s

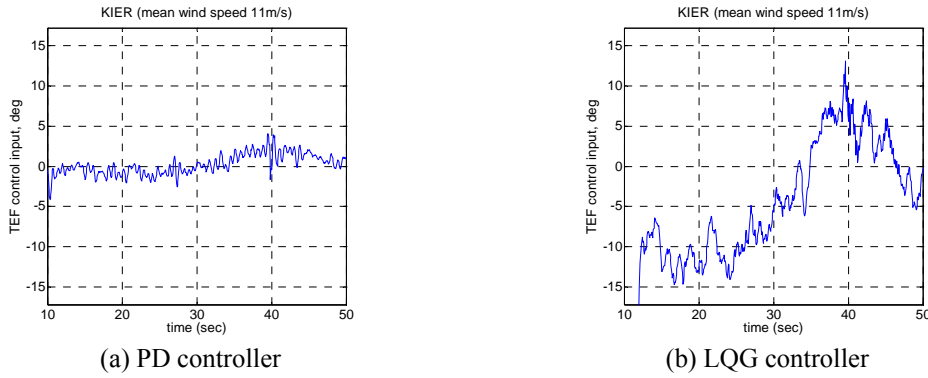


Fig. 11 TEF control input of the KIER model at wind speed 11 m/s

Table 4 STD results of the NREL model

Controller	Mean (kNm)	STD (kNm) (no control → controlled)	Reduction (%)
PID	7850	685 → 485	29
LQG	7850	675 → 412	39

Table 5 STD results of the KIER model

Simulation case	Mean (kNm)	PID controller (kNm)	Reduction (%)	Mean (kNm)	LQG controller (kNm)	Reduction (%)
7 m/s, 11 rpm	1000	162 → 106	35	950	143 → 76	47
11 m/s, 15.7 rpm	2400	285 → 169	41	2250	254 → 123	51
15 m/s, 15.7 rpm	1400	295 → 274	8	1250	284 → 227	20

5. Conclusions

This study investigated the use of trailing edge flaps for the load reduction of large wind turbine blades. The aeroelastic analysis method used in this study is composed of a wind turbine blade structural model based on a flexible multibody dynamics and an unsteady aerodynamic model based on the modified strip theory. The TEF is modeled in the aeroelastic analysis method using the thin airfoil theory without actuator dynamics. The control performance of the TEFs was examined for the NREL and KIER wind turbines. The PD and LQG controllers were used to control the trailing edge flap angle, and both control strategies were shown to be effective for load reduction. However, the LQG controller necessitates a better performing TEF actuator than the PD controller. Through numerical simulations that use the trailing edge flaps as active aerodynamic load control devices on wind turbines, a reduction of 30-50% in the standard deviation of the root bending moment oscillations was achieved. This translates to a reduction in the fatigue damage on the wind turbines, resulting in maintenance cost reductions.

Acknowledgements

This work was supported by the New & Renewable Energy of the Korea Institute of Energy Technology Evaluation and Planning (KETEP) grant funded by the Korea government Ministry of Knowledge Economy (Contract No. 2009T100100253).

References

- Andersen, P.B., Gaunaa, M., Bak, C. and Buhl, T. (2007), "Wind tunnel test on wind turbine airfoil with adaptive trailing edge geometry", *Proceedings of the 45th AIAA aerospace sciences meeting and exhibition*, Reno, NV, USA.
- Barlas, T.K. and Kuik, van G.A.M. (2009), *Aeroelastic modelling and comparison of advanced active flap control concepts for load reduction on the upwind 5MW wind turbine*, DUWIND, Delft University of Technology.
- Basualdo, S. (2005), "Load alleviation on wind turbine blades using variable airfoil geometry", *Wind Eng.*, **29**(2), 169–182.
- Bergami, L. (2008), *Aeroservoelastic Stability of a 2D airfoil section equipped with a trailing edge flap*, Technical report, Riso-R-1663(EN).
- DeLaurier, J.D. (1993), "An aerodynamic model for flapping-wing flight", *Aeronaut. J.*, **97**, 125-130.
- Dorato, P. and Abdallah, C. (1995), *Linear-quadratic control: an introduction*, Prentice Hall, New Jersey, Chap. 2, 6.
- Gaunaa, M. (2006), *Unsteady 2D potential-flow forces on a thin variable geometry airfoil undergoing arbitrary motion*, Technical report, Risø-R-1478 (EN).
- Holm-Jørgensen, K., Stærdahl, J.W. and Nielsen, S.R.K. (2008), "On the nonlinear structural analysis of wind turbine blades using reduced degree-of-freedom models", *Struct. Eng. Mech.*, **28**(1), 107-127.
- Jonkman, J., Butterfield, S., Musial, W. and Scott, G. (2009), *Definition of a 5MW reference wind turbine for offshore system development*, Technical report NREL/TP-500-38060.
- Kim, D.K., Lee, J.S. and Han, J.H. (2011), "Improved aerodynamic model for efficient analysis of flapping-wing flight", *AIAA J.*, **49**(4), 868-872.
- Ljung, L. (2001), "Prediction error estimation methods", *Circ. Syst. Signal Pr.*, **21**(1), 11-21.
- Ogata, K. (1990), *Modern control engineering*, 2nd Ed, Prentice-Hall International Editions.

- Soderstrom, T. and Stoica, P. (1989), *System identification*, Prentice Hall, UK, Chap. 5, 7.
- Theodorsen, T. (1935), *General theory of aerodynamic instability and the mechanism of flutter*, NACA Report 496.
- Troldborg, N. (2005), "Computational study of the RisøB1-18 airfoil with a hinged flap providing variable trailing edge geometry", *Wind Eng.*, **29**(2), 89–113.
- Wilson, D.G., Berg, D.E., Barone, M.F., Berg, J.C., Resor, B.R. and Lobitz, D.W. (2009), *Active aerodynamic blade control design for load reduction on large wind turbines*, European Wind Energy Conference & Exhibition 2009, Parc Chanot, Marseille, France.

CC